





RESEARCH ARTICLE | NOVEMBER 15 2023

Dissociation of ultracold cesium Rydberg-ground molecules



Jingxu Bai; Yuechun Jiao  ; Rong Song; Zhenhua Li; Jianming Zhao  ; Suotang Jia



J. Chem. Phys. 159, 194302 (2023)

<https://doi.org/10.1063/5.0175109>



View
Online



Export
Citation

CrossMark

Dissociation of ultracold cesium Rydberg-ground molecules

Cite as: J. Chem. Phys. 159, 194302 (2023); doi: 10.1063/5.0175109

Submitted: 5 September 2023 • Accepted: 23 October 2023 •

Published Online: 15 November 2023



View Online



Export Citation



CrossMark

Jingxu Bai,¹ Yuechun Jiao,^{1,2,a)}  Rong Song,¹ Zhenhua Li,¹ Jianming Zhao,^{1,2,a)}  and Suotang Jia^{1,2}

AFFILIATIONS

¹State Key Laboratory of Quantum Optics and Quantum Optics Devices, Institute of Laser Spectroscopy, Shanxi University, Taiyuan 030006, People's Republic of China

²Collaborative Innovation Center of Extreme Optics, Shanxi University, Taiyuan 030006, People's Republic of China

^{a)}Authors to whom correspondence should be addressed: ycjiao@sxu.edu.cn and zhaojm@sxu.edu.cn

ABSTRACT

We report the experimental measurements of the decay rate of polar cesium $nD_{5/2} - 6S_{1/2}$ Rydberg-ground molecules with a large principal quantum number range of $35 \leq n \leq 40$. Rydberg molecules are prepared employing the method of two-photon photoassociation and the molecular (atomic) ions, due to autoionization (blackbody photoionization), are detected with a microchannel plate detector. The decay rate Γ of the vibrational ground state of the deep and shadow bound molecules for triplet ($^T\Sigma$) and mixed singlet-triplet ($^{S,T}\Sigma$) are measured by fitting the molecular population with the exponential function. Comparing with the parent atom, the decay rate of the polar Rydberg-ground molecule shows an obvious increase with a magnitude of a few μs . The possible dissociation mechanism of polar Rydberg-ground molecules including a collisional decay, blackbody induced decay, and coupling of adjacent Rydberg states and tunneling decay are discussed in detail. The theoretical model is induced to simulate the measurements, showing agreement.

Published under an exclusive license by AIP Publishing. <https://doi.org/10.1063/5.0175109>

I. INTRODUCTION

Rydberg molecules, consisting of one or more Rydberg atoms, have become an attractive research field since they were first predicted in theory,^{1,2} and observed in experiment,^{3,4} due to their exotic binding mechanism. Usually, Rydberg molecules are divided into three types according to the different binding mechanisms. The first one is the Rydberg-Rydberg molecule, also called a Rydberg macrodimer, that is formed by a pair of atoms both being Rydberg states.^{2,4-7} The binding mechanism of Rydberg macrodimer comes from the electrical multipole interaction between Rydberg atoms. The second one is the Rydberg-ground molecule, formed with one Rydberg-state atom and one ground-state atom.^{3,8-19} The binding mechanism of the Rydberg-ground molecule comes from the scattering interaction of a Rydberg electron with a neutral atom, often described with Fermi pseudopotential. The third is a novel kind of ion-Rydberg molecule consisting of one ion and a Rydberg atom, where the corresponding binding mechanism is the long-range monopole and electric multipole interaction. This kind of molecule is proposed in theory^{20,21} and observed in experiment in Rb.²² Due to the large size ($\sim\mu\text{m}$) and huge permanent electric

dipole moment (\sim kilo-Debye), Rydberg-ground molecules have been investigated with different angular quantum number of Rydberg states and different atomic samples, such as alkali atoms Rb nS ,^{3,8} nP ,¹⁴ and nD ¹⁰⁻¹² state, Cs atoms nS ,¹³ nP ,¹⁴ and nD ,¹⁵⁻¹⁸ and alkaline-earth Sr atom Rydberg-ground molecules.¹⁹

In addition to the properties of large size and permanent dipole moment, the decay and dissociation of Rydberg molecules are other important characteristics. As we know, Rydberg atoms have long lifetime scaling as n^3 (n is the principal quantum number). For example, the calculated spontaneous radiation decay rate of Cs $60D_{5/2}$ state is 8.06 kHz, and the effective decay rate at 300 K accounting for the blackbody radiation effect is about 13.16 kHz. For the Rydberg-ground molecule, it has a similar short decay rate compared to the corresponding atomic Rydberg state. In Ref. 23, Butscher *et al.* investigated the decay rate and corresponding lifetime of $^T\Sigma(5S - 35S)$ long-range Rb₂ Rydberg molecules in the vibrational ground state and an excited state, which demonstrated that the molecular decay rate is much faster than that of corresponding Rydberg atoms. The decay rate of $^T\Sigma(5S - 35S)$ state shows atomic density dependence. Camargo *et al.*²⁴ also investigated the decay rate of ultra-long-range strontium Rydberg molecules, the

corresponding decay rate of the low-lying vibrational states being very similar to those of the parent Rydberg atoms where the related lifetime is on the order of dozen microseconds.

In this work, we present the measurement of decay rate of polar cesium $nD_{5/2} - 6S_{1/2}$ ($n = 35 - 40$) Rydberg-ground molecules. We prepare the D -type Rydberg-ground molecule employing the two-photon photoassociation technique, and obtain the Rydberg molecular signal for different interaction time, t_D . The decay rates of the Rydberg molecules for a triplet $^T\Sigma$ and a mixed singlet-triplet $^{S,T}\Sigma$ of $v = 0$ vibration state are extracted by an exponential fitting of molecules signals. We find that decay rates of cesium $nD_{5/2} - 6S_{1/2}$ are much faster than that of the corresponding parent Rydberg atoms, which is different from rubidium²³ and strontium²⁴ Rydberg-ground molecules. On the basis of the measured decay rate, we qualitatively discuss and analyze molecular dissociation mechanisms and possible decay channels.

II. EXPERIMENTAL SCHEME

The experiment is carried out in a crossed optical dipole trap (CODT) loaded from a magneto-optical trap (MOT), where the chamber vacuum pressure is 2×10^{-7} Pa. The detail of the experiments is reported elsewhere.¹⁶ The CODT density, measured with an absorption imaging method, is orders of 10^{11} cm^{-3} , which is sufficiently dense for exciting Rydberg-ground molecules with bond lengths ≈ 0.12 μm (our case). In experiments, the two-photon photoassociation scheme is employed to achieve the Rydberg excitation, displayed in Fig. 1(a). The first-photon laser (852 nm) drives the lower transition $6S_{1/2}(F = 4) \rightarrow 6P_{3/2}(F' = 5)$ with the frequency blue detuned $\delta = +360$ MHz from the intermediate $6P_{3/2}$ state. Meanwhile the second-photon laser (510 nm) achieves the Rydberg transition $6P_{3/2} \rightarrow nD_{5/2}$. Two photoassociation lasers with a beam waist of 80 μm (852 nm) and 40 μm (510 nm) are overlapped in a counter propagating geometry through the atom cloud in the MOT center, the schematic of experimental apparatus is shown in Fig. 1(b). The frequency of first-photon laser is locked with a polarization spectroscopy²⁵ technique and the second-photon laser is stabilized to an ultra-stable Fabry-Perot (F-P) cavity with a fineness of 15 k employing Pound-Drever-Hall (PDH) technique, corresponding laser linewidth less than 100 kHz. A pair of grids on either side of the atomic cloud along y -axis are used for applying the potential and driving atomic and molecular ions to MCP detector. The other two pairs of grids along x - and z -axis, not shown here, are used to compensate stray electric field, related the stray field around the cold cloud is expected to be less than 20 mV/cm.

For attaining the Rydberg molecular spectra, we scan the second-photon 510 nm laser frequency from the atomic Rydberg line to red 150 MHz detuning by scanning the radio-frequency signal (rf) applied to the electro-optic modulator (EOM) that is employed to lock the laser to the FP cavity. Rydberg molecules are formed when the detuning from the atomic line matches the binding energy of a molecular vibrational state. The ions of Rydberg molecular (atomic) due to the Hornbeck-Molnar autoionization (blackbody photoionization) are detected with a MCP detector.

The decay rate of the Rydberg molecule can be extracted by analyzing the molecular signal as a function of the delay time t_D , see Fig. 1(c). We investigate the density dependence of Rydberg molecular decay rates by changing the time interval t_M between MOT beam

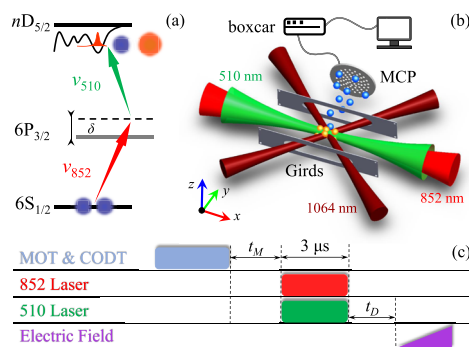


FIG. 1. (a) Two-photon excitation diagram of Rydberg state. The first-photon ν_{852} (red arrow) laser drives the lower transition $6S_{1/2} \rightarrow 6P_{3/2}$ with the frequency 360 MHz blue detuned from the intermediate $6P_{3/2}$ state. The second-photon ν_{510} (green arrow) laser achieves the Rydberg excitation of $6P_{3/2} \rightarrow nD_{5/2}$, preparing Rydberg atoms and Rydberg-ground molecules. (b) Sketch of experimental setup. Two excited lasers are counter-propagated through the MOT center along the x -direction. Ions of molecules (atoms) due to Hornbeck-Molnar autoionization (blackbody photoionization) are detected with a MCP detector and processed with a boxcar and recorded with a computer. (c) Timing sequence. After switching off the MOT and CODT beam, we turn on two-photon excitation pulse with duration 3 μs for preparing Rydberg atoms and molecules. The electric field is switched on for ions acceleration and detection after a time delay of t_D . The time interval, t_M , is used to change the MOT density.

and Rydberg excitation beams and further changing atomic density, see Fig. 1(c). It is found that the nice two-photon photoassociation spectroscopy in the MOT can be obtained for higher n , such as $n = 38$ and 39. However for lower n , the molecular spectra are attained only in the CODT.

III. DECAY RATE OF RYDBERG MOLECULES

The binding energy of Rydberg-ground molecule comes from the scattering interaction of the Rydberg electron and the ground-state atom. We firstly calculate the potential curves and vibrational energies of cesium $nD_{5/2} - 6S_{1/2}$ Rydberg-ground molecules based on the Fermi pseudopotential model,^{26,27} which have been reported in detail in previous work.^{12,16-18} In Fig. 2(a), we present the calculations of the potential energy curves of cesium $37D_{5/2} - 6S_{1/2}(F = 4)$ Rydberg-ground molecule. The potential curves are asymptotically related to the $37D_{5/2}$ atomic line. The outermost wells of $R > 1900a_0$ mainly arise from the s -wave scattering interaction forming trilobite-type Rydberg-ground molecules, whereas the inner wells of $R < 1900a_0$ on the order of GHz mainly from the p -wave scattering forming butterfly-type Rydberg-ground molecules. In this work, we focus on the outermost bound potential wells with dozens of megahertz deep at $R \approx 2200a_0$.

As described in our previous work,¹⁶⁻¹⁸ the potential curves of Fig. 2(a) include two potential wells, the deep triplet $^T\Sigma$ (blue) and shallow mixed $^{S,T}\Sigma$ (red) wells. To understand fully the features of Rydberg-ground molecules, in Fig. 2(a) we also present the vibration wave functions of $v = 0$ state for $^{S,T}\Sigma$ (red) and $^T\Sigma$ (blue), calculated with the molecular Hamiltonian theory.

In Fig. 2(b), we display measured two-photon photoassociation spectrum for $37D_{5/2}$ Rydberg state. The black circles are the

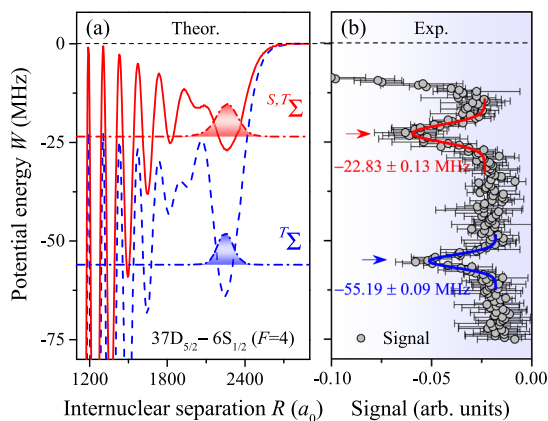


FIG. 2. (a) Calculations of potential energy curves of $37D_{5/2} - 6S_{1/2} (F=4)$ Rydberg-ground molecule asymptotically related to the $37D_{5/2}$ atomic line. The deep potential curve (blue dashed line) indicates a triplet $T\Sigma$ state and shallow potential curve (red solid line) is a hyperfine mixed singlet-triplet $S,T\Sigma$ state. In the outermost wells, the color filled dashed-curves display the vibrational wave functions of ($v=0$) state. (b) Measurement of the two-photon photoassociation spectroscopy of the $37D_{5/2} - 6S_{1/2} (F=4)$ Rydberg-ground molecule. The red and blue solid curves are Gaussian fittings to the molecular peaks yielding a peak center of -22.83 ± 0.13 MHz for $S,T\Sigma$ and -55.19 ± 0.09 MHz for $T\Sigma$, respectively. The error bars are the standard average errors of five independent measurements.

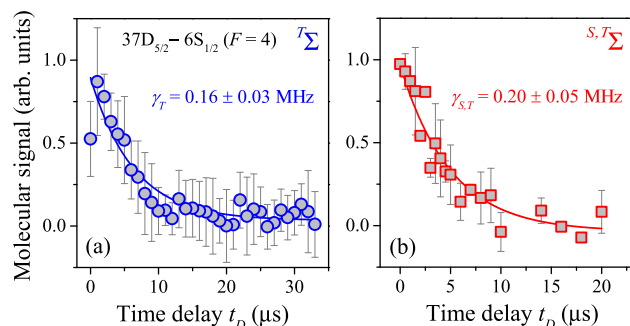


FIG. 3. Normalized signal of $37D_{5/2} - 6S_{1/2}$ molecule as a function of the time delay t_D for $T\Sigma$ state (a) and $S,T\Sigma$ state (b). The solid lines are the exponential fittings yielding decay rate of $\gamma_T = 0.16 \pm 0.03$ MHz and $\gamma_{S,T} = 0.20 \pm 0.05$ MHz, respectively.

ionic signals and error bars are the standard average errors of five independent measurements. The zero detuning displays $37D_{5/2}$ Rydberg atomic line. It is clearly seen that there are two peaks in red detuned sides that are distributed to Rydberg-ground molecular signals. These two peaks are attributed to the vibrational ground state $v=0$ of $T\Sigma$ (blue) and $S,T\Sigma$ (red) molecular states, corresponding binding energies are -55.19 ± 0.09 and -22.83 ± 0.13 MHz, respectively. The measurement shows a good agreement with the calculation in Fig. 2(a). The relative deviations are less than 3%, which are originating from the laser linewidth and frequency calibration.

TABLE I. Measured decay rates in MHz, $\gamma_{S,T}$ and γ_T , of $nD_{5/2} - 6S_{1/2}$ molecules in their vibrational ground state. The error bars display the fitting errors of exponential function. The forth column lists calculations of spontaneous emission decay rates γ_0 of $nD_{5/2}$ parent Rydberg atoms.

n	$\gamma_{S,T}$	γ_T	γ_0
35	0.17 ± 0.05	0.11 ± 0.06	0.044
37	0.20 ± 0.05	0.16 ± 0.03	0.037
38	0.23 ± 0.04	0.16 ± 0.04	0.034
39	0.29 ± 0.05	0.19 ± 0.03	0.031
40	0.31 ± 0.04	0.19 ± 0.20	0.029

In order to obtain the decay rate of Rydberg-ground molecule, we do a series of measurements like in Fig. 2(b) for different time delay, t_D . From the Gaussian fittings to the molecular peaks, we attain the molecular signal strength (proportional to the molecular number) as a function of the time delay t_D , as shown in Fig. 3(a) for $T\Sigma$ and Fig. 3(b) for $S,T\Sigma$ state. The decay rates are extracted to be $\gamma_T = 0.16 \pm 0.03$ MHz and $\gamma_{S,T} = 0.20 \pm 0.05$ MHz by exponential fitting to the measurements of Fig. 3.

We have done more decay rate measurements for $n=35-40$, the decay rate of $nD_{5/2} - 6S_{1/2}$ molecules are displayed in the Table I. The decay rates, both γ_T and $\gamma_{S,T}$, demonstrate slightly increasing with principal quantum number n . For comparison, we also present the spontaneous emission decay rate of corresponding parent Rydberg atoms in the forth column of the Table I.

IV. DISCUSSIONS

It is found that, from the Table I, the decay rate γ_T of the triplet state is smaller than $\gamma_{S,T}$ of the mixed state. We attribute this to: (i) the potential well of $T\Sigma$ state is deeper than that of $S,T\Sigma$ state, showing more stable and stronger binding than $S,T\Sigma$ state; (ii) the tunneling decay rate of $T\Sigma$ state is less than that of $S,T\Sigma$ state, which will be discussed later. We also found that the decay rates of both Rydberg-ground molecule are significantly faster compared to their parent Rydberg atoms. The decay rate of Rydberg-ground molecule is about 3–4 times for $n=35$ and 6–10 times for $n=40$ faster than that of the related parent atoms.

In order to make the discussion more convenient, in Table II, we present the measured lifetimes for $\tau_{S,T}$ and τ_T , of $nD_{5/2} - 6S_{1/2}$

TABLE II. Measured lifetimes in μs , $\tau_{S,T}$ and τ_T , of $nD_{5/2} - 6S_{1/2}$ molecules in their vibrational ground state. The error bars display the fitting errors of exponential function. The forth column displays calculations of spontaneous emission lifetimes τ_0 of $nD_{5/2}$ parent Rydberg atoms.

n	$\tau_{S,T}$	τ_T	τ_0
35	6.04 ± 1.70	9.32 ± 4.39	22.5
37	5.01 ± 1.25	6.30 ± 1.09	26.9
38	4.30 ± 0.64	6.27 ± 1.50	29.4
39	3.39 ± 0.56	5.16 ± 0.82	31.9
40	3.18 ± 0.39	5.17 ± 3.26	34.6

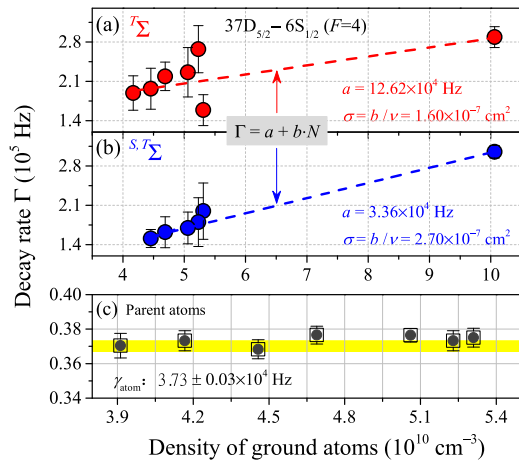


FIG. 4. Measured decay rate Γ of molecular state ${}^7\Sigma(v=0)$ state (a) and ${}^{5,7}\Sigma(v=0)$ (b) as a function of the ground-atom density for $37D_{5/2}$ Rydberg state. For comparison, we also display the decay rates of the parent atom γ_{atom} in (c). Red and blue dashed lines display the fittings of function $\Gamma = a + bN$ to the data. The yellow shadow in (c) means the average atomic decay rate.

molecules in their vibrational ground state $\nu = 0$ and the spontaneous emission lifetimes of parent Rydberg atoms. In the following, we discuss the decay and dissociation mechanism and possible decay channels of Rydberg-ground molecules. The possible decay channels include the decay due to the autoionization of molecules, ground-state atomic collision, and blackbody induced transition, and decay to nearby bind state and so on.

We first discuss the decay channel due to the ground-state atomic collision, $\Gamma_{col} = bN = N\sigma v$, with N the atomic density, b the fitting parameter, σ the collision cross section, and v the mean velocity of the atom. For the temperature of MOT atom about $100 \mu\text{K}$, the mean velocity $v \approx 10 \text{ cm/s}$. In order to obtain the decay rate dependence on the ground-state density, we measure the decay rate ($\Gamma = 1/\tau$) of $37D_{5/2} - 6S_{1/2}$ molecular vibrational ground state for different atomic density by varying the t_M , as shown in Fig. 4(a) for ${}^7\Sigma$ and (b) for ${}^{5,7}\Sigma$ states. (Atomic density is monitored by absorption imaging). It is shown that the decay rate exhibits nearly linear increases with the atomic density. Using the function $\Gamma = a + bN$, we fit the data of Figs. 4(a) and 4(b), displayed with dashed lines. The fitting yields the cross section $\sigma = b/v = 1.60 \times 10^{-7}$ and $2.70 \times 10^{-7} \text{ cm}^2$ for ${}^7\Sigma$ and ${}^{5,7}\Sigma$ state, respectively. The measurements of cross section shows reasonable agreement with the geometric collision section $\sim 3 \times 10^{-7} \text{ cm}^2$, calculated with the formula $\sigma_{theor.} = \pi r^2$ with $r \sim 3 \mu\text{m}$. In addition, the fitting also yields a parameter $a = 12.62 \times 10^4$ and $3.36 \times 10^4 \text{ Hz}$, for ${}^7\Sigma$ and ${}^{5,7}\Sigma$ state, which displays decay rate due to the other decay channels discussed below.

Secondly, we discuss the decay rate due to the blackbody radiation. Analogous to the atomic Rydberg state, the molecules can decay radiatively to a pair of free atoms due to the blackbody effect, and the related decay process is written as

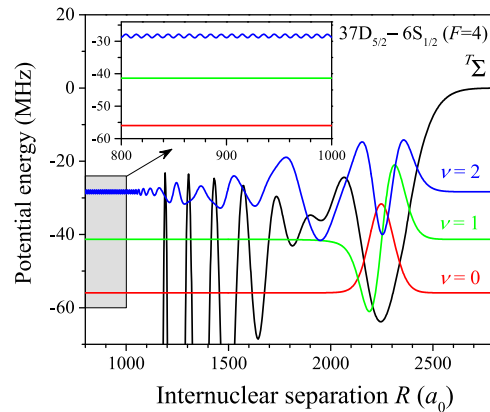
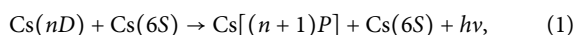


FIG. 5. Calculated potential energy curve (black) and vibrational wavefunction for $\nu = 0$ (red), 1 (green), 2 (blue) of ${}^7\Sigma$ of $36D_{5/2} - 6S_{1/2}$ ($F = 4$). Inset is the enlargement of the gray shallow region.

where ν is the frequency of microwave photon of transition $nD \rightarrow (n+1)P$. The effect induced with blackbody on decay rate is similar for Rydberg-ground molecule and for the relative parent Rydberg atom.³ Here we estimate the effect of blackbody on molecular decay by calculating the natural decay rate γ_0 and effective decay accounting blackbody for parent Rydberg atom γ_{eff} . For instance, the calculated natural decay rate of $37D_{5/2}$ state is $\gamma_0 = 37.2 \text{ kHz}$ and effective decay rate at 300 K is $\gamma_{eff} = 49.8 \text{ kHz}$. In experiment, the measured natural decay rate of $37D_{5/2}$ state is $37.3 \pm 0.6 \text{ kHz}$, which is in agreement with the calculation. In Fig. 4(c) we present the decay rate measurement of $37D_{5/2}$ state as a function of the atomic density, which displays that the atomic decay rate is independent on atomic density⁸ at the low density case.

We thirdly discuss the decay due to the tunneling. The tunneling is the quantum phenomenon where a wavefunction can propagate through a potential barrier, whose related transmission rate depends on the barrier height and barrier width. As shown in Fig. 5, we calculated the vibrational wavefunctions of $\nu = 0$ (red), 1 (green), 2 (blue) for ${}^7\Sigma$ state of $36D_{5/2} - 6S_{1/2}$ ($F = 4$). We can obviously see that many inner potentials are deeper than the outermost potentials, which means the vibrational wavefunction can tunnel through these inner potentials. The tunneling decay rate generated from flux model is written as

$$\Gamma_{tunnel} = (|A|^2 k \hbar / M) / P_0, \quad (2)$$

where Γ_{tunnel} is the tunneling decay rate in $1/s$, P_0 is the normalized integral of Ψ over the trapped region (unitless), A is the amplitude of the (real-valued) sinusoid for ψ in the scattering region in $1/\sqrt{m}$, and k is the wavenumber in the scattering region in $1/m$, and M is the effective mass in kg. Seeing the enlargement of the gray shallow in Fig. 5, for $\nu = 0, 1$, the amplitude A of the sine-like wave-function in the scattering region at $R = 1000a_0$ or less is almost zero, suggesting that the tunneling decay rate can be neglected. On the contrary, for $\nu = 2$, the calculated Γ_{tunnel} is about 1000 kHz which results the rapidly decay for Rydberg-ground molecule.

The Breit-Wigner function is another method for extracting a tunneling decay rate from static wavefunction amplitudes whose

formula is written as, $\Gamma = (2/\hbar)(dW/d\Phi)$, with W the energy in Nm, and Φ the scattering phase in rads. This gives Gamma in units frequency. This is the $(1/e)$ decay rate divided by 2π . It would be equivalent to the spectroscopic linewidth in Hz. The $1/e$ decay rate is $\Gamma_{decay} = (2/\hbar)(dW/d\Phi)$. Note the \hbar in place of just h . For our case, the tunneling decay rate from the above two models have essentially given the same information that, for the molecule $v = 0$ we prepared, the tunneling effect is not a major reason that results the rapidly decay.

Finally, we discuss the decay to nearby bind state, related decay rate depending on the Franck-Condon factor (G_{FC}). However, a set of vibrational states builds a basis of normalized eigenstates, the sum of the Franck-Condon factor,

$$\sum_{v'} G_{FC}[nDv \rightarrow n'Pv'] = 1. \quad (3)$$

According to the discussion above, we can conclude that the collision and blackbody reduced decays are the main reason that result the fast decay of the Rydberg-ground molecules. To fully understand the decay mechanism, we take the $^S,T\Sigma$ state of $37D_{5/2} - 6S_{1/2}$ molecules as an example to quantitatively display the decomposition of the decay rate. The collision cross section is $\sigma = 2.70 \times 10^{-7} \text{ cm}^2$ from Fig. 4(b), the decay rate due to the collision is 141.21 kHz at the density of $N = 5.23 \times 10^{10} \text{ cm}^{-3}$. Whereas the decay rate due to the blackbody radiation of the parent atom is about 37.33 kHz. From the Fig. 5, the amplitude of the sine-like wavefunction in the scattering region at less than $R = 2000 a_0$ is almost zero, related tunneling decay rate is zero. The total decay rate is consistent with the experimental measurement of 179.96 kHz.

V. SUMMARY

In this work, we have presented measurements of decay rates of cesium $nD_{5/2} - 6S_{1/2}$ ($F = 4$) Rydberg-ground molecules for $35 \leq n \leq 40$. The Rydberg-ground molecules are prepared in the Rydberg ensemble by the method of two-photon photoassociation. We have obtained the molecular decay rate by means of fitting the measured population of molecules as a function of the time delay between the excitation pulse and the detection electric field. The decay rates of Rydberg molecule show increase with the principal quantum number and on the order of hundreds of kHz, which is much larger than that of their parent Rydberg atoms.

We have discussed possible decay channels in details, including autoionization induced decay of molecules, blackbody induced decay, the tunneling induced decay and collision between atoms induced decay. We found that the measured decay rate of the Rydberg-ground molecules shows the linear increase with atomic density, while the related bare Rydberg atoms are independent of the atomic density at lower atomic density. From the linear fitting, we have extracted the cross section that agrees with the calculation.

Among the possible decay channels, the ground-state atomic collision and the blackbody radiation of the parent Rydberg atom are the important decay channels, which can lead to the significant increase of the molecular decay rate. Decay mechanism is an important property both for Rydberg atom and for molecules, which plays a key role in atomic and molecular physics. The measurements of decay rate and the exploration of decay mechanisms are of great

significance for understanding the binding mechanisms of Rydberg molecules.

ACKNOWLEDGMENTS

We thank Professor G. Raithel for valuable discussions on the calculation of the potential and experiments. This work is supported by the National Natural Science Foundation of China (Grant Nos. 12120101004, 12241408, 61835007, and 62175136); the Scientific Cooperation Exchanges Project of Shanxi province (Grant No. 202104041101015); the Changjiang Scholars and Innovative Research Team in Universities of the Ministry of Education of China (Grant No. IRT 17R70), and Grant No. 1331 project of Shanxi province.

AUTHOR DECLARATIONS

Conflict of Interest

The authors have no conflicts to disclose.

Author Contributions

Jingxu Bai: Data curation (equal); Formal analysis (equal); Investigation (equal); Software (equal); Visualization (equal); Writing – original draft (equal). **Yuechun Jiao:** Conceptualization (equal); Funding acquisition (equal); Writing – review & editing (equal). **Rong Song:** Data curation (equal); Investigation (equal). **Zhenhua Li:** Software (equal); Visualization (equal). **Jianming Zhao:** Conceptualization (equal); Funding acquisition (equal); Project administration (equal); Supervision (equal); Writing – review & editing (equal). **Suotang Jia:** Project administration (equal); Supervision (equal).

DATA AVAILABILITY

The data that support the findings of this study are available from the corresponding authors upon reasonable request.

REFERENCES

- C. H. Greene, A. S. Dickinson, and H. R. Sadeghpour, "Creation of polar and nonpolar ultra-long-range Rydberg molecules," *Phys. Rev. Lett.* **85**, 2458–2461 (2000).
- C. Boisseau, I. Simbotin, and R. Côté, "Macrodimers: Ultralong range Rydberg molecules," *Phys. Rev. Lett.* **88**, 133004 (2002).
- V. Bendkowsky, B. Butscher, J. Nipper, J. P. Shaffer, R. Löw, and T. Pfau, "Observation of ultralong-range Rydberg molecules," *Nature* **458**, 1005–1008 (2009).
- K. R. Overstreet, A. Schwettmann, J. Tallant, D. Booth, and J. P. Shaffer, "Observation of electric-field-induced Cs Rydberg atom macrodimers," *Nat. Phys.* **5**, 581–585 (2009).
- J. Deiglmayr, H. Saßmannshausen, P. Pillet, and F. Merkt, "Observation of dipole-quadrupole interaction in an ultracold gas of Rydberg atoms," *Phys. Rev. Lett.* **113**, 193001 (2014).
- H. Saßmannshausen and J. Deiglmayr, "Observation of Rydberg-atom macrodimers: Micrometer-sized diatomic molecules," *Phys. Rev. Lett.* **117**, 083401 (2016).

- ⁷X. Han, S. Bai, Y. Jiao, L. Hao, Y. Xue, J. Zhao, S. Jia, and G. Raithel, “Cs $62D_J$ Rydberg-atom macrodimers formed by long-range multipole interaction,” *Phys. Rev. A* **97**, 031403(R) (2018).
- ⁸V. Bendkowsky, B. Butscher, J. Nipper, J. B. Balewski, J. P. Shaffer, R. Löw, T. Pfau, W. Li, J. Stanojevic, T. Pohl, and J. M. Rost, “Rydberg trimers and excited dimers bound by internal quantum reflection,” *Phys. Rev. Lett.* **105**, 163201 (2010).
- ⁹M. A. Bellos, R. Carollo, J. Banerjee, E. E. Eyler, P. L. Gould, and W. C. Stwalley, “Excitation of weakly bound molecules to trilobitelike Rydberg states,” *Phys. Rev. Lett.* **111**, 053001 (2013).
- ¹⁰D. A. Anderson, S. A. Miller, and G. Raithel, “Photoassociation of long-range nD Rydberg molecules,” *Phys. Rev. Lett.* **112**, 163201 (2014).
- ¹¹A. T. Krupp, A. Gaj, J. B. Balewski, P. Ilzhöfer, S. Hofferberth, R. Löw, T. Pfau, M. Kurz, and P. Schmelcher, “Alignment of D -state Rydberg molecules,” *Phys. Rev. Lett.* **112**, 143008 (2014).
- ¹²J. L. MacLennan, Y.-J. Chen, and G. Raithel, “Deeply bound ($24D_J + 5S_{1/2}$) ^{87}Rb and ^{85}Rb molecules for eight spin couplings,” *Phys. Rev. A* **99**, 033407 (2019).
- ¹³J. Tallant, S. T. Rittenhouse, D. Booth, H. R. Sadeghpour, and J. P. Shaffer, “Observation of blueshifted ultralong-range Cs_2 Rydberg molecules,” *Phys. Rev. Lett.* **109**, 173202 (2012).
- ¹⁴H. Saßmannshausen, F. Merkt, and J. Deiglmayr, “Experimental characterization of singlet scattering channels in long-range Rydberg molecules,” *Phys. Rev. Lett.* **114**, 133201 (2015).
- ¹⁵C. Fey, J. Yang, S. T. Rittenhouse, F. Munkes, M. Baluktsian, P. Schmelcher, H. R. Sadeghpour, and J. P. Shaffer, “Effective three-body interactions in $\text{Cs}(6s)\text{-Cs}(nd)$ Rydberg trimers,” *Phys. Rev. Lett.* **122**, 103001 (2019).
- ¹⁶S. Bai, X. Han, J. Bai, Y. Jiao, J. Zhao, S. Jia, and G. Raithel, “Cesium $nD_J + 6S_{1/2}$ Rydberg molecules and their permanent electric dipole moments,” *Phys. Rev. Res.* **2**, 033525 (2020).
- ¹⁷S. Bai, X. Han, J. Bai, Y. Jiao, H. Wang, J. Zhao, and S. Jia, “Observation of photoassociation spectroscopy of ultralong $37D_{5/2} + 6S_{1/2}$ Cs_2 Rydberg molecules,” *J. Chem. Phys.* **152**, 084302 (2020).
- ¹⁸S. Y. Bai, J. X. Bai, X. X. Han, Y. C. Jiao, J. M. Zhao, and S. T. Jia, “Observation of cesium ($nD_{5/2} + 6S_{1/2}$) ultralong-range Rydberg-ground molecules,” *Chin. Phys. Lett.* **37**, 123201 (2020).
- ¹⁹J. D. Whalen, F. Camargo, R. Ding, T. C. Killian, F. B. Dunning, J. Pérez-Ríos, S. Yoshida, and J. Burgdörfer, “Lifetimes of ultralong-range strontium Rydberg molecules in a dense Bose-Einstein condensate,” *Phys. Rev. A* **96**, 042702 (2017).
- ²⁰A. Duspayev, X. Han, M. A. Viray, L. Ma, J. Zhao, and G. Raithel, “Long-range Rydberg-atom-ion molecules of Rb and Cs,” *Phys. Rev. Res.* **3**, 023114 (2021).
- ²¹M. Deiß, S. Haze, and J. Hecker Denschlag, “Long-range atom-ion Rydberg molecule: A novel molecular binding mechanism,” *Atoms* **9**, 34 (2021).
- ²²N. Zuber, V. Anasuri, M. Berngruber, Y. Q. Zou, F. Meinert, R. Löw, and T. Pfau, “Observation of a molecular bond between ions and Rydberg atoms,” *Nature* **605**, 453–456 (2022).
- ²³B. Butscher, V. Bendkowsky, J. Nipper, J. B. Balewski, L. Kukota, R. Löw, T. Pfau, W. Li, T. Pohl, and J. M. Rost, “Lifetimes of ultralong-range Rydberg molecules in vibrational ground and excited states,” *J. Phys. B: At., Mol. Opt. Phys.* **44**, 184004 (2011).
- ²⁴F. Camargo, J. D. Whalen, R. Ding, H. R. Sadeghpour, S. Yoshida, J. Burgdörfer, F. B. Dunning, and T. C. Killian, “Lifetimes of ultra-long-range strontium Rydberg molecules,” *Phys. Rev. A* **93**, 022702 (2016).
- ²⁵C. P. Pearman, C. S. Adams, S. G. Cox, P. F. Griffin, D. A. Smith, and I. G. Hughes, “Polarization spectroscopy of a closed atomic transition: Applications to laser frequency locking,” *J. Phys. B: At., Mol. Opt. Phys.* **35**, 5141–5151 (2002).
- ²⁶E. Fermi, “Sopra lo spostamento per pressione delle righe elevate delle serie spettrali,” *Nuovo Cimento* **11**, 157–166 (1934).
- ²⁷A. Omont, “On the theory of collisions of atoms in Rydberg states with neutral particles,” *J. Phys. France* **38**, 1343–1359 (1977).